A phased array applicator based on open ridged-waveguide antenna for microwave hyperthermia

Received: 20 July 2021

DOI: 10.1002/mop.33039

WILEY

RESEARCH ARTICLE

A phased array applicator based on open ridged-waveguide antenna for microwave hyperthermia

Morteza Ghaderi Aram[1] | **Hadi Aliakbarian**[2] | **Hana Dobšíček Trefná**[1]

[1]Department of Electrical Engineering, Chalmers University of Technology, Gothenburg, Sweden

[2]Faculty of Electrical Engineering, K. N. Toosi University of Technology, Tehran, Iran

Correspondence
Morteza Ghaderi Aram, Department of Electrical Engineering, Chalmers University of Technology, 412 96 Gothenburg, Sweden.
Email: aramg@chalmers.se

Abstract

Radiative hyperthermia is a clinically applied cancer treatment modality where antenna design is crucial to achieving therapeutic goals. Serving as the building block of a phased-array configuration, antennas are typically arranged in a cylindrical or elliptical array called applicator. This short communication proposes an elliptical phased array applicator based on a compact, UWB design from the category of double-ridged horn antennas customized for hyperthermia systems. The performance of the antenna, named open ridged-waveguide, has been experimentally assessed based on the quality metrics of the hyperthermic community. The proposed design achieves an ultra-wideband range of operation from 400 to 800 MHz with an aperture size of 3 by 4 cm. Moreover, thanks to the shielding provided by the metallic housing, the design proves good isolation better than −30 dB throughout the band. The power deposition capability of the proposed applicator followed by the thermal analysis is also investigated for a realistic head and neck patient model. The results indicate very good quality metrics achieved in the treatment planning of the patient.

KEYWORDS

beamforming, phased array applicators, specific absorption rate, UWB antennas

1 | INTRODUCTION

During the past couple of decades, antennas have found various applications in biomedical engineering, leading to a growing branch of research called bio-electromagnetics (BioEM). BioEM includes, but is not limited to, microwave imaging[1] and hyperthermia (HT).[2] The aim of HT is to increase the efficacy of routine cancer treatment modalities, such as radiotherapy and chemotherapy, by targeting focused EM energy at the tumors under treatment. This selective targeting gives a mild rise to tumor's temperature (of about 5–7°C above the normal body temperature), and as a result, enhances the drug absorption in the tumor.[3]

Devices for heating up the target tissue are called applicators in the HT context. Dealing with lossy human tissues, an appropriate antenna for HT applicators needs to operate in the lower part of the UHF band to penetrate deeply enough into the body. This is because the penetration depth falls rapidly at higher frequencies. This also means that a matching medium, commonly referred to as water bolus, between the antenna and the body is needed to not only facilitate the wave transition into the body but also to prevent the heating of the body surface.[4] In general, an ideal antenna design for HT is directive and compact and preferably has a symmetrical radiation pattern with a reflection coefficient better than −10 dB throughout a wide frequency band of operation.

For deep HT treatments, several antennas are typically arranged in a cylindrical or elliptical configuration.[4] A variety of antenna types for this purpose have been already proposed in the literature.[5–7] However, they either suffer from a very narrow frequency bandwidth or need an RF matching network/balun to achieve a symmetrical radiation field and stable electrical performance. Besides making the antenna larger and more complex, matching networks absorb a substantial amount of power and thus decrease the efficiency of these designs. Therefore, in terms of reliability and reproducibility, antennas in which an RF matching network can

be avoided have a clear advantage when used for a clinical treatment.[5]

Furthermore, the optimum phase and amplitude of each element in the array need to be determined so that the focal point is steered on the target and that hot-spot formations in the healthy tissue are suppressed. Several beamforming methods have been proposed in the literature among which we count the generalized eigenvalue problem,[8] time reversal (TR),[9,10] particle swarm optimization (PSO),[11] and focusing via constrained optimization.[12]

This study proposes an elliptical phased array applicator for deep HT that uses a new antenna model from the double-ridged horn family.[13] The antenna, henceforth called open ridged-waveguide (ORWG), has a UWB characteristic and requires no matching network or balun.[14] To assess the efficacy of the proposed applicator, the treatment planning of a realistic head and neck (H&N) patient model is investigated. As far as the SAR-based beamforming of the plan is concerned, a hybrid TR-PSO beamforming method is proposed to minimize the cost function by taking advantage of TR fast computation and using it as the starting point. For the thermal analysis, an open-source computational platform, called FEniCS,[15] is used.

2 | MATERIALS AND METHODS

2.1 | ORWG design

The ORWG antenna, whose design and optimization procedures are given elsewhere,[14] is a water-filled and compressed version of a conventional double-ridged horn antenna. The different parts of the antenna are visualized in Figure 1, and their dimensions are as follows (all in centimeter): $a = 3.7$, $b = 3$, $L_1 = 2.3$, $L_2 = 0.3$, $G = 1$, $h = 0.75$, $w_1 = 3.18$, and $w_2 = 3.3$.

2.2 | Antenna measurement setup

Two ORWG antennas were fabricated, and a thin rubber diaphragm was attached to their apertures to act as a lid. Separating the antenna from the surface bolus, this lid made it possible for the water to circulate inside the structure through a small inlet and outlet. Experimental verification was performed in a standardized setup with a muscle tissue load as described in HT quality assurance guidelines[16,17] and depicted in Figure 2A.

A hydrogel bolus[18] with the dimensions of $36 \times 16 \times 3$ cm was placed on top of a muscle phantom with dimensions $36 \times 25 \times 6$ cm. Consisting of 99% water and 1% polymer, a hydrogel bolus is a convenient solution with the potential to replace water-filled plastic bags in HT procedures. The relative permittivities and conductivities of the hydrogel and muscle phantom were assessed by Agilent 85070E dielectric probe kit and shown in Figure 2B,C, respectively.

2.3 | Patient model and the phased array applicator

A realistic patient model of a 34-year-old man called Duke[19] with a tumor in the tongue region was investigated. The model, shown in Figure 3A, was segmented by a trained radiation oncologist and the tumor was then inserted into it. The voxel model consists of 45 tissue types whose thermal and dielectric properties are taken from the IT'IS database[20] at 500 MHz. To form a phased array applicator for the treatment planning of this model, 16 ORWG antennas were arranged in an elliptical configuration which has two rings with an inter-ring distance of 5 cm. Shown in Figure 3B is the antenna placement around the patient model simulated in CST Microwave Studio.[21] The water bolus was modeled using the first-order Debye model in CST (Figure 3C) and its major axis, minor axis, and height are 14, 11, and 14 cm, respectively.

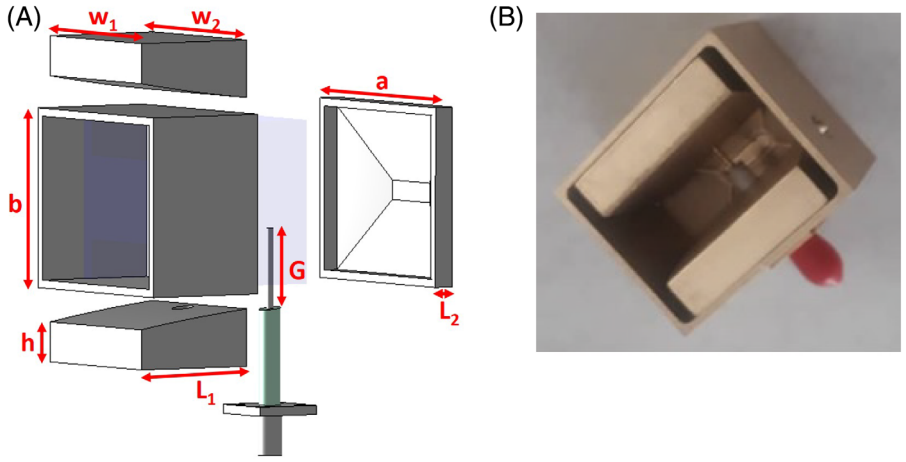

FIGURE 1 The open ridged-waveguide antenna. (A) Its different parts and parameters (the blue shade shows water inside the structure). (B) The fabricated model [Color figure can be viewed at wileyonlinelibrary.com]

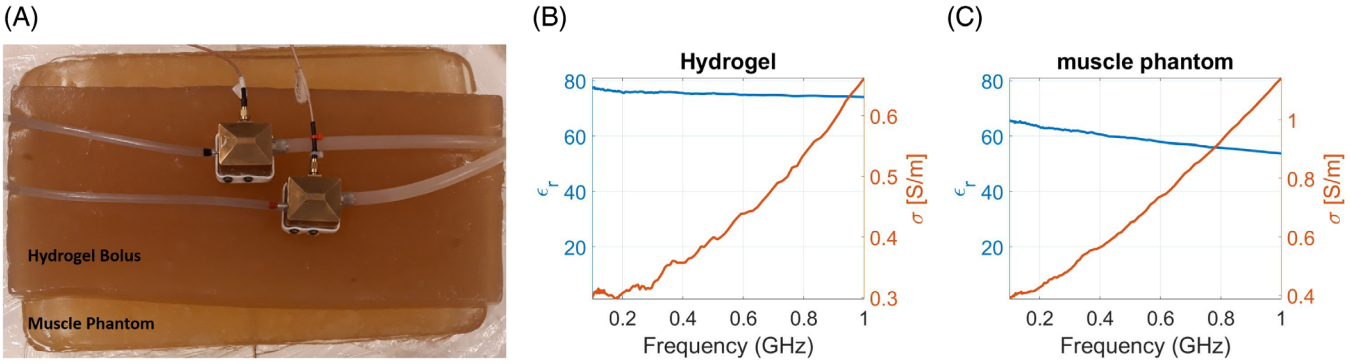

FIGURE 2 Hyperthermia (HT) standardized setup. (A) Two fabricated open ridged-waveguide (ORWG) antennas on top of a flat hydrogel bolus and a muscle phantom. (B) and (C) Are the measured dielectric properties of the hydrogel and muscle phantom, respectively [Color figure can be viewed at wileyonlinelibrary.com]

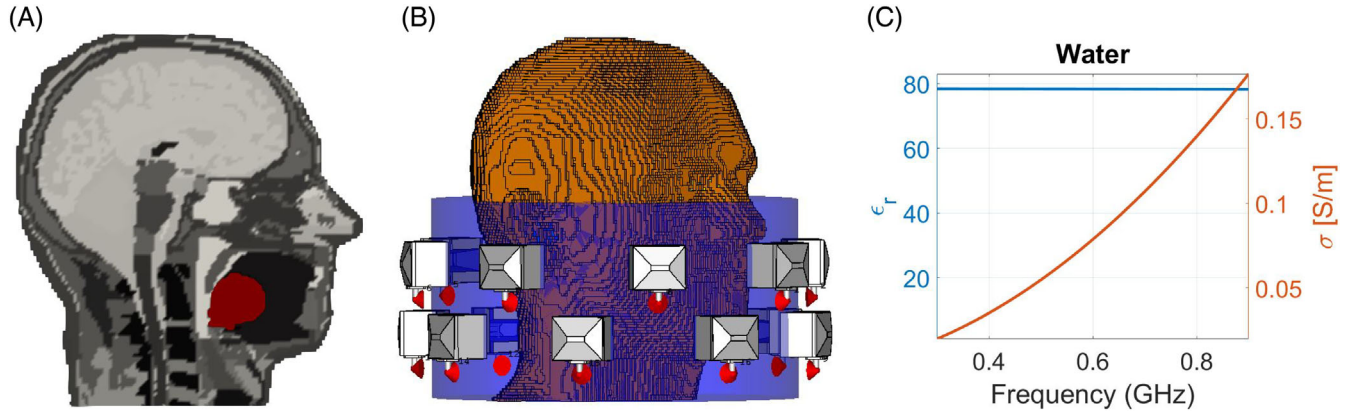

FIGURE 3 (A) Cross-section of the patient model with a large tumor shown in red in the tongue region. (B) CST model of the patient along with a 16-element elliptical array of open ridged-waveguide (ORWG) antennas and (C) the dielectric properties of the first-order Debye model of water used in the simulation [Color figure can be viewed at wileyonlinelibrary.com]

2.4 | SAR beamforming

Implementation of PSO in EM problems is straightforward. A thorough discussion about it and about how to choose its parameters is given by Robinson et al.[22] The main steps taken in this process are listed below which also include the integration of the TR technique in the initialization phase of the PSO algorithm.

- Definition of the problem space: 15 particles were set to search the solution space of a unit circle in the complex plane. So each particle was a 16 by one vector of complex numbers in that space.
- Initialization of the 1st swarm: TR setting was assigned to the first particle in the set because we wanted to take advantage of having a good initial guess.
- *Cost function*: Hotspot-tumor quotient (HTQ) was selected as the cost function in this study as follows

$$\mathrm{HTQ} = \frac{\overline{\mathrm{SAR}}(V_{1\%})}{\overline{\mathrm{SAR}}(T)} \tag{1}$$

where $\overline{\mathrm{SAR}}(V_{1\%})$ and $\overline{\mathrm{SAR}}(T)$ are the highest percentile of SAR distribution in the healthy tissue and the mean SAR absorbed by the tumor, respectively.

- Termination condition: the optimization was terminated when the maximum number of iterations (M) or the maximum number of stall iterations (S) was reached, whichever came first. In this problem, M and S were set to 30 and 5, respectively.

2.5 | Bioheat equation and thermal simulation

The deposited EM energy in terms of power loss density (PLD) eventually turns into heat due to the Joule heating effect. Because of blood circulation in body, biological models involve perfused tissues. Taking into account the blood perfusion rate, the simplest way to model this phenomenon is by using Pennes Bioheat equation[23] as follows:

$$c_p \rho \frac{\partial T}{\partial t} = \nabla \cdot (k \nabla T) + PLD - c_b w_b (T - T_b) \tag{2}$$

where $T\,(^{\circ}\mathrm{C})$ is temperature; $\rho\,(\mathrm{kg/m^3})$ is mass density; $c_p\,(\mathrm{J/^{\circ}C/kg})$ is heat capacity; $k\,(\mathrm{W/^{\circ}C/m})$ is thermal conductivity; and T_b, c_b, and $w_b\,(\mathrm{kg/m^3/s})$ are temperature, heat capacity, and perfusion rate of blood, respectively.

While one can go for commercial solvers like CST and Comsol to tackle such a multi-physics problem to some extent, we believe that a modular, open-source computational engine provides more flexibility to model, simulate, and optimize the phenomenon. It can also save a lot of computational time upon efficient implementation. Hence after exporting the EM field from CST, we chose to perform the thermal simulation with a powerful FEM-based computational engine called FEniCS.[15] Tetrahedron mesh generation for the solver was done by Iso2mesh,[24] an open-source MATLAB/Octave-based package.

3 | RESULTS

Figure 4A shows the measured S_{11} and S_{21} of the fabricated ORWG antennas. The setup for this measurement was according to Figure 2A. As can be seen from the black solid line, the return loss of the design remains below −10 dB from 375 to 815 MHz; a bandwidth of 440 MHz. Moreover, as shown with the solid blue line in this plot, the two antennas placed in the close vicinity of each other have a low level of mutual coupling, less than −35 dB throughout the whole band.

The return loss and cross-talk among the adjacent elements of the phased array applicator of Figure 3B are shown in Figure 4B. As can be seen, the design's characteristic (S_{11}) for this realistic scenario is slightly different from the S_{11} measured when the antenna was in front of a flat muscle

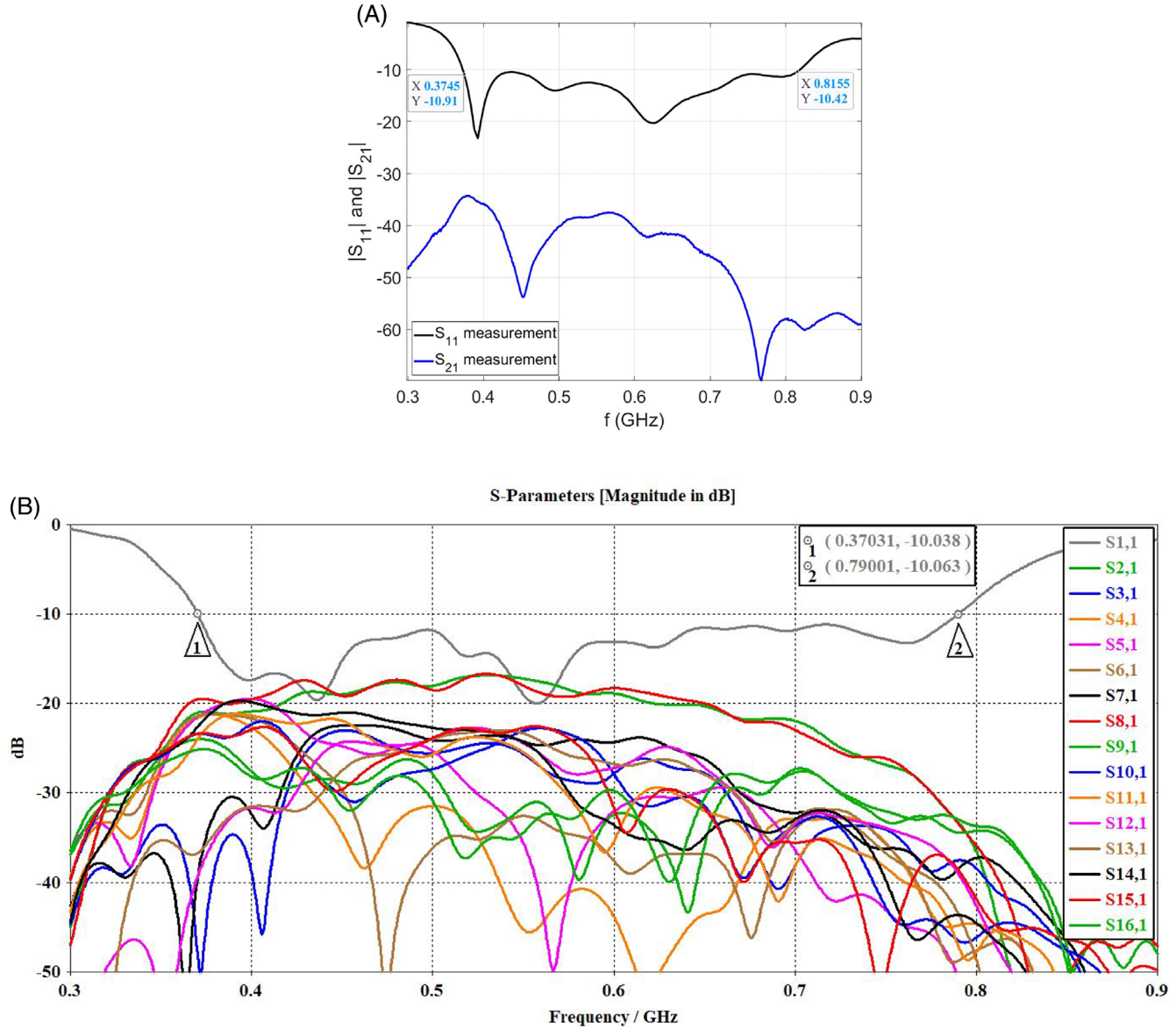

FIGURE 4 (A) Measured return loss and the mutual coupling between the two elements shown in Figure 2A. (B) Simulated return loss and the cross-talk between the 16 elements in the array configuration of Figure 3B [Color figure can be viewed at wileyonlinelibrary.com]

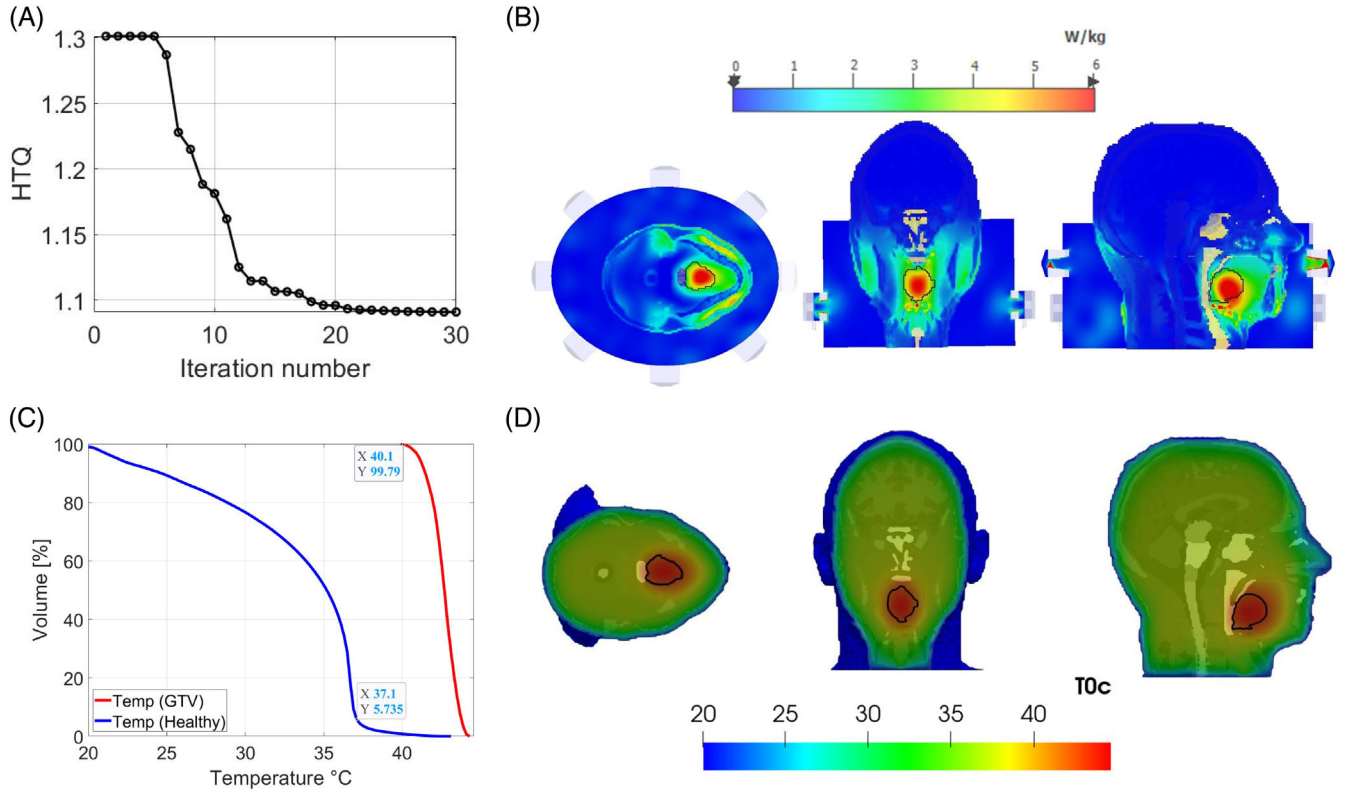

FIGURE 5 (A) Time reversal–particle swarm optimization (TR-PSO) for minimization of the Hotspot-tumor quotient (HTQ) at 500 MHz. (B) Point SAR distributions for the normalized excitation power of 0.5 W per channel in transverse, coronal, and sagittal planes, from left to right respectively and (C) temperature–volume histograms for the steady-state distribution both in Gross Tumor Volume (red line) and in the healthy tissue (blue line). (D) Temperature distributions in the corresponding planes (tumor's outline is shown by the solid black line) [Color figure can be viewed at wileyonlinelibrary.com]

phantom. This was expected due to the variation of water bolus thickness resulting from the natural body curvature. However, the design still enjoys a very good return loss below −10 dB within the desired band. Another interesting observation is that the plot shows a higher level of cross-talk among elements arranged in an elliptical configuration than the level already recorded between those placed on top of a flat muscle phantom. According to Figure 4B, when the first antenna acts as the transmitter, the highest level of mutual coupling happens to its immediate neighboring elements, that is, antennas number 2 and 8 in the top ring.

Figure 5A shows the cost function minimization at 500 MHz using the TR-PSO method. The HTQ indicator of TR is 1.3 which was used to initialize the PSO routine for further optimization. It is almost axiomatic that using an educated initial guess can not only help to reduce the optimization time in an otherwise lengthy process (typically more than 100 iterations), but it can also lower the odds of getting trapped in local minima. This hybrid routine resulted in the final value of 1.09 for the HTQ in less than 25 iterations (the five last iterations were the stall iterations as discussed in Section 2.4). Regarding the computational cost, the whole optimization process on an ordinary laptop with an Intel Corei7® CPU of 2.8 GHz took around 260 s to converge.

The resultant point SAR distribution of the optimized plan along with the temperature distribution are shown in Figure 5B, D in transverse, coronal, and sagittal planes, respectively. The normalized excitation power per channel was 0.5 W by default in CST. After beamforming, the amplification factor for the combined PLD used in the thermal analysis was set to be 10 to raise the maximum temperature up to 44°C. As can be seen, the tumor's coverage is very good with no significant hotspot in the healthy tissue. Plus, some quantified metrics for the thermal analysis are depicted in Figure 5C. Temperature–volume histogram in this sub-figure indicates that almost the whole volume of tumor has a temperature above 40°C at the steady-state phase while only less than 6% of the healthy tissue volume experiences a temperature higher than the normal body temperature during the treatment. Observe that the $T < 37$°C is caused by the fixed temperature of the bolus (20°C) applied as Dirichlet boundary condition to the patient skin. To quantify the quality of the treatment outcome based on commonly used metrics in the HT community, SAR treatment quantifier of target coverage 25% (TC_{25}) and thermal indicators of T_{90}, T_{50}, T_{10} were measured as follows: $TC_{25} = 97\%$, $T_{90} = 41.8$°C, $T_{50} = 43$°C, and $T_{10} = 43.9$°C. TC_{25} indicates the percentage of the tumor volume that is enclosed by the iso-contour

of 25% of the maximum deposited SAR in the tumor. Similarly, the thermal indicator of T_x determines the temperature in the target tumor exceeding by x percent of all the temperature values. Obviously, the larger the TC_{25} and T_x, the better the treatment quality.

4 | CONCLUSIONS

A new antenna model, recently proposed for HT applications, was further investigated in this study. An elliptical phased array applicator hiring 16 ORWG antennas was analyzed in the treatment planning of an H&N patient. Both the characteristics of the antenna and the treatment outcome of the plan are very good and satisfactory. This motivates further development and implementation of the proposed applicator for clinical applications.

CONFLICT OF INTEREST

The authors declare no conflict of interests.

DATA AVAILABILITY STATEMENT

Data sharing is not applicable to this article as no new data were created or analyzed in this study.

ORCID

Morteza Ghaderi Aram https://orcid.org/0000-0003-2073-6966
Hadi Aliakbarian https://orcid.org/0000-0001-5257-3423

REFERENCES

[1] Pastorino M. *Microwave Imaging*. John Wiley & Sons; 2010:208.

[2] Hand JW, Hynynen K, Shrivastava P, Saylor T. *Methods of External Hyperthermic Heating*. Springer Science & Business Media; 2012.

[3] Kampinga HH. Cell biological effects of hyperthermia alone or combined with radiation or drugs: a short introduction to newcomers in the field. *Int J Hyperthermia*. 2006;22(3):191-196.

[4] Paulides M, Bakker J, Neufeld E, et al. The HYPERcollar: a novel applicator for hyperthermia in the head and neck. *Int J Hyperthermia*. 2007;23(7):567-576.

[5] Paulides MM, Bakker JF, Chavannes N, Van Rhoon GC. A patch antenna design for application in a phased-array head and neck hyperthermia applicator. *IEEE Trans Biomed Eng*. 2007;54(11):2057-2063.

[6] Zweije R, Kok HP, Bakker A, Bel A, Crezee J. Technical and clinical evaluation of the ALBA-4D 70MHz loco-regional hyperthermia system. *IEEE*. 2018;328-331. https://doi.org/10.23919/EuMC43975.2018

[7] Takook P, Persson M, Gellermann J, Trefná HD. Compact self-grounded Bow-Tie antenna design for an UWB phased-array hyperthermia applicator. *Int J Hyperthermia*. 2017;33(4):387-400.

[8] Köhler T, Maass P, Wust P, Seebass M. A fast algorithm to find optimal controls of multiantenna applicators in regional hyperthermia. *Phys Med Biol*. 2001;46(9):2503.

[9] Trefná HD, Vrba J, Persson M. Time-reversal focusing in microwave hyperthermia for deep-seated tumors. *Phys Med Biol*. 2010;55(8):2167.

[10] Rahimi F, Chamaani S. Applying a repetitive time-reversal method to reduce input power of a wearable hyperthermia applicator for breast cancer treatment. *Microw Opt Technol Lett*. 2020;62(12):3754-3766.

[11] Nguyen PT, Abbosh AM, Crozier S. 3-D focused microwave hyperthermia for breast cancer treatment with experimental validation. *IEEE Trans Antennas Propag*. 2017;65(7):3489-3500.

[12] Bellizzi GG, Crocco L, Battaglia GM, Isernia T. Multi-frequency constrained SAR focusing for patient specific hyperthermia treatment. *IEEE J Electromagn RF Microw Med Biol*. 2017;1(2):74-80.

[13] Mehrdadian A, Fallahi H, Kaboli M, Mirtaheri SA. Design and implementation of 0.7 to 7 GHz broadband double-ridged horn antenna. *IEEE*. 2014;250-255. https://doi.org/10.1109/IST34122.2014

[14] Aram MG, Aliakbarian H, Trefna HD. The open ridged-waveguide antenna: an ultra-wideband, compact design for hyperthermia applicators. *Phys Med Biol*. 2021.

[15] Alnæs M, Blechta J, Hake J, et al. The FEniCS project version 1.5. *Arch Numer Soft*. 2015;3(100):9-23.

[16] Trefná HD, Crezee J, Schmidt M, et al. Quality assurance guidelines for superficial hyperthermia clinical trials. *Strahlenther Onkol*. 2017;193(5):351-366.

[17] Trefná HD, Crezee H, Schmidt M, et al. Quality assurance guidelines for superficial hyperthermia clinical trials: I. Clinical requirements. *Int J Hyperth*. 2017;33(4):471-482.

[18] Trefná HD, Ström A. Hydrogels as a water bolus during hyperthermia treatment. *Phys Med Biol*. 2019;64(11):115025.

[19] Christ A, Kainz W, Hahn EG, et al. The virtual family—development of surface-based anatomical models of two adults and two children for dosimetric simulations. *Phys Med Biol*. 2009;55(2):N23.

[20] Hasgall P, Di Gennaro F, Baumgartner C, et al. *IT'IS Database for Thermal and Electromagnetic Parameters of Biological Tissues*. IT'IS Foundation; 2018.

[21] CST. *CST Microwave Studio Advanced Topics*. Technical Reports; 2019.

[22] Robinson J, Rahmat-Samii Y. Particle swarm optimization in electromagnetics. *IEEE Trans Antennas Propag*. 2004;52(2):397-407.

[23] Wissler EH. Pennes' 1948 paper revisited. *J Appl Physiol*. 1998;85(1):35-41.

[24] Fang Q, Boas DA. Tetrahedral mesh generation from volumetric binary and grayscale images. *IEEE*. 2009;1142-1145. https://doi.org/10.1109/ISBI.2009.5193259

How to cite this article: Aram MG, Aliakbarian H, Trefná HD. A phased array applicator based on open ridged-waveguide antenna for microwave hyperthermia. *Microw Opt Technol Lett*. 2021;1–6. https://doi.org/10.1002/mop.33039